

## New measures of multimodality for the detection of a ghost stochastic resonance

H. Braun,<sup>1,2</sup> P. Ditlevsen,<sup>1</sup> and J. Kurths<sup>3,4</sup>

<sup>1</sup>Centre for Ice and Climate, Niels Bohr Institute, University of Copenhagen, Juliane Maries Vej 30, 2100 Copenhagen, Denmark

<sup>2</sup>Heidelberg Academy of Sciences and Humanities, Im Neuenheimer Feld 229, 69120 Heidelberg, Germany

<sup>3</sup>Institute of Physics, Humboldt University Berlin, Newtonstraße 15, 12489 Berlin, Germany

<sup>4</sup>Potsdam Institute for Climate Impact Research, P.O. Box 60 12 03, 14412 Potsdam, Germany

(Received 16 September 2009; accepted 25 November 2009; published online 29 December 2009)

Large-amplitude (10–15 K) millennial-duration warming events, the Dansgaard–Oeschger (DO) events, repeatedly occurred in the North Atlantic region during ice ages. So far, the trigger of these events is not known. To explain their recurrence pattern, a ghost stochastic resonance (GSR) scenario has been suggested, i.e., a dynamical scenario in which the events represent the subharmonic response to centennial-scale solar forcing plus noise. According to this hypothesis a multimodal phase distribution of the events is expected, which should be tested on the basis of climate records by means of time series analysis. A major obstacle in these tests, however, is the need of a statistical measure of regularity that can distinguish between a random occurrence of DO events and a GSR scenario. Here we construct and compare three new measures of phase multimodality. In a Monte Carlo simulation with a simple conceptual model of DO events we simulate probability distributions of the measures under both scenarios for realizations of only 11 DO events. Based on these distributions we find that our measures are able to distinguish between a random occurrence and a GSR scenario. We further apply our measures to analyze the recurrence pattern of the last 11 DO events in the North Greenland Ice Core Project deep ice core from Greenland. © 2009 American Institute of Physics. [doi:10.1063/1.3274853]

Nontrivial effects of noise in nonlinear systems have been a classical topic for many years. It is established that noise can even play a constructive role in synchronizing various types of nonlinear dynamical systems. The mechanisms of stochastic resonance (SR) and coherence resonance (CR) are probably the most prominent examples of this fact. Recent work focused on the mechanism of ghost stochastic resonance (GSR). In this mechanism, a stochastic nonlinear dynamical system, with two quasistationary states, is forced by at least two periodic input cycles. It has been demonstrated that for an optimal noise level the output of the system can be synchronized at the fundamental frequency  $1/T$  of the forcing (where  $T$  denotes the period of the cyclic input), that is, at a frequency with zero input power. This is in contrast to the usual SR, in which the output is synchronized at the same frequency as the forcing. It has further been shown that in a GSR scenario, a multimodal recurrence pattern of output events can be expected. For time series analysis, this recurrence pattern poses a major challenge since it highlights the need to develop more efficient measures of complex, nonperiodic regularity, which are difficult to construct. Here we use a simple two-state dynamical model with a threshold to develop new measures of multimodality, which may be used to distinguish between a GSR and a scenario of solely noise-induced events. We use these measures in a Monte Carlo approach to analyze the recurrence pattern of large-amplitude (10–15 K), shiftlike anomalies in glacial climate, the Dansgaard–Oeschger (DO) events, which are documented, for ex-

ample, in deep ice core records from Greenland. So far, the cause of these remarkable glacial climate oscillations is still unknown. Using our method we find a recurrence pattern of DO events which might be explained by a GSR scenario. We expect that our methodological advance should be of value for future studies, in which the statistical significance of the detected recurrence pattern needs to be tested.

### I. INTRODUCTION

Many paleoclimatic time series show the existence of millennial-scale warming events during ice ages, the DO events (Dansgaard *et al.*, 1982; Grootes *et al.*, 1993; Bond *et al.*, 1993), cf. Fig. 1. The temperature variations during these events were estimated to be on the order of 10–15 K, as can be deduced from the ratio of stable isotopes in deep ice cores from Greenland (Severinghaus and Brook, 1999; Lang *et al.*, 1999). DO events are commonly interpreted as oscillations between two different states of operation of glacial climate, the stadial (=cold) and the interstadial (=warm) state, respectively (Dansgaard *et al.*, 1982; Oeschger *et al.*, 1984; Broecker *et al.*, 1985; Sarnthein *et al.*, 1994; Alley and Clark, 1999; Steffensen *et al.*, 2008). These two states could correspond to two fundamentally different modes of the Atlantic ocean circulation, a cold mode with buoyancy deep convection south of the Greenland–Scotland ridge, and a warm mode with buoyancy deep convection north of the ridge (Ganopolski and Rahmstorf, 2001), cf. Fig. 2. Buoyancy deep

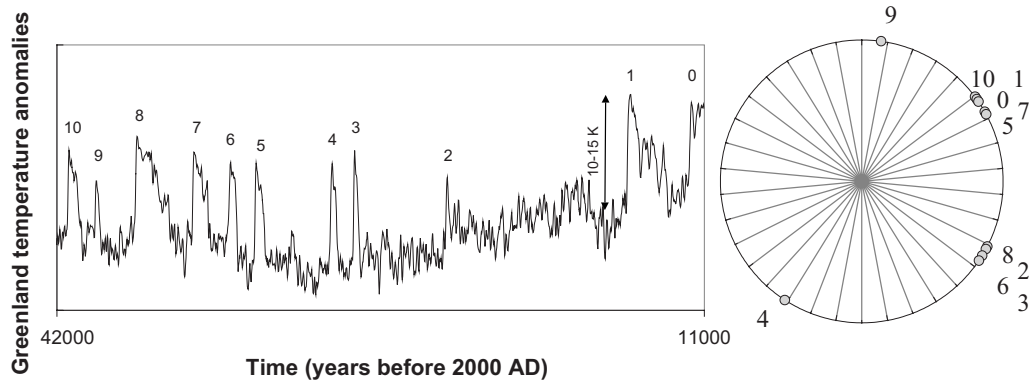


FIG. 1. DO events 0–10 as seen in the NGRIP deep ice core from Greenland during the time interval between 11 000 and 42 000 yr before present (Andersen *et al.*, 2006; Svensson *et al.*, 2006). Left: time domain. The timing of the onset of the DO events is given in Table I. Right: phase domain. The figure shows the timing  $t_n$  of the onset of the events, plotted on the unit circle using the transformation  $\phi_n = 2\pi t_n / 1487.5$ , where  $\phi_n$  denotes the phase of the events. Note that the unit circle in the right part is divided into 34 sectors to better illustrate the cluster of the observed at a few values (“modes”) of  $\phi_n$ .

convection is a threshold process, since it occurs when the density of the surface water becomes larger than the density of the deep ocean water. From a dynamical system viewpoint, DO events can thus be regarded as repeated oscillations between two fundamentally different states of operation in a system with a threshold and with a millennial time scale (Alley *et al.*, 2003).

So far, it is still not agreed upon if DO events are purely random or synchronized by some external (e.g., solar) forcing. For the “pro-synchronization,” see Alley *et al.* (2001), Schulz (2002), Rahmstorf (2003), Braun *et al.* (2005), and Braun (2009). For the “con-synchronization,” see Ditlevsen *et al.* (2005), Ditlevsen *et al.* (2007), and Ditlevsen and

Ditlevsen (2009) (note that a general description of the concept of synchronization is given, for example, in Boccaletti *et al.*, 2002). In this discussion, a GSR mechanism has been suggested, i.e., a dynamical scenario in which DO events are triggered by a combination of noise plus centennial-scale solar forcing in cycles of about  $1470/7$  ( $\approx 210$ ) and  $1470/17$  ( $\approx 86.5$ ) yr (Braun *et al.*, 2008). These cycles closely match the leading centennial-scale spectral components of solar variability as deduced from various solar and solar-terrestrial time series, such as the sunspot record, auroral records, and tree ring based  $^{14}\text{C}$  records (Feynman and Fougere, 1984; Stuiver and Braziunas, 1993; Peristykh and Damon, 2003).

However, distinguishing between a GSR scenario and a scenario of solely noise-induced DO events on the basis of only about 10–20 sufficiently well-dated DO events is challenging: in a GSR scenario a nonperiodic recurrence pattern of DO events is expected, i.e., a multimodal phase distribution, which resembles the phase distribution of the DO events 0–10 in the North Greenland Ice Core Project (NGRIP) ice core from Greenland (right part in Fig. 1). Standard measures of periodicity are thus not efficient to detect a GSR scenario, as has explicitly been shown (Braun, 2009). Here we construct three measures of phase multimodality. Using a simple model for the dynamics of DO events, we explicitly demonstrate that these measures are able to distinguish between a random occurrence of DO events and two simplified GSR model scenarios, with a known forcing period, on the basis of just 11 DO events. We further apply our measures to analyze the recurrence pattern of DO events in the NGRIP deep ice core from Greenland and we find a pattern that is consistent with a GSR scenario. We note, however, that we are not yet able to estimate the statistical significance of the detected recurrence pattern. This results from the fact that the forcing period in the suggested GSR scenario is not exactly known, for example, due to the existence of uncertainties in the solar cycle periods and in the ice core chronology. Therefore, our approach to calculate the statistical significance in the model simulations needs to be further elaborated to be applicable to the observed DO events in the ice core records. This elaboration, however, requires an even

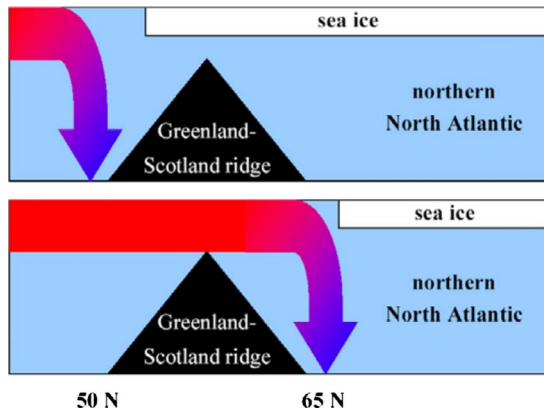


FIG. 2. (Color online) Two modes of operation of the Atlantic Ocean circulation during DO events, as suggested by Ganopolski and Rahmstorf (2001). Top: cold (stadial) mode. Bottom: warm (interstadial) mode. In both modes, warm surface water from lower latitudes flows northward to the North Atlantic and cools due to heat exchange with the colder atmosphere. Near the sea ice margin the cooling is sufficiently strong to enable sinking of surface water to the deep ocean (deep buoyancy convection). In the cold mode, this process occurs south of the Greenland-Scotland ridge, whereas it occurs north of the ridge in the warm mode. As a result, sea ice reaches as far as about 50 north in the cold mode, but only to about 65 north in the warm mode. Because sea ice has a strong atmospheric cooling effect, this difference between both oceanic modes is expected to result in strong differences in North Atlantic surface air temperature, similar to DO events. Since the density of water depends on salinity, transitions between both modes can be triggered, for example, by anomalies in the surface freshwater flux to the North Atlantic.

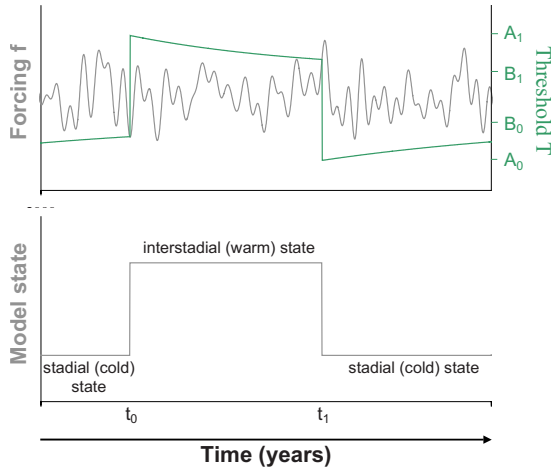


FIG. 3. (Color online) Dynamics of DO events in the two-state model. Top: forcing  $f$  (thin curve) and threshold function  $T$  (thick curve). Bottom: model state. A switch from the stacial (cold) to the interstadial (warm) state is triggered when the forcing falls below the threshold function (at time  $t_0$  in the figure). During this switch, which is interpreted as the beginning of a DO event in the model, the threshold function takes a nonequilibrium value ( $A_1$ ) and then approaches its new equilibrium value  $B_1$  following a millennial scale relaxation process with relaxation time  $\tau_1$ . The opposite switch, which terminates a DO event in the model, takes place when the forcing exceeds the threshold function (at time  $t_1$  in the figure). Again, the threshold function takes a nonequilibrium value ( $A_0$ ) and then approaches its new equilibrium value  $B_0$  following another millennial scale relaxation process with relaxation time  $\tau_0$ . All model parameters are given in Table II.

more advanced statistical treatment, which is beyond the scope of this paper.

## II. A SIMPLE TWO-STATE MODEL OF DO EVENTS

Defining a statistical measure that is able to distinguish between a scenario of solely noise-induced DO events and a GSR scenario clearly requires the identification of characteristic recurrence patterns in a GSR scenario. For that purpose we use a simple dynamical model of DO events, which has been deduced from the dynamics of DO events in a much more sophisticated ocean-atmosphere model (Braun *et al.*, 2005; Braun *et al.*, 2007). An extensive description of the simple model was given by Braun *et al.* (2007), including a discussion of its geophysical motivation, its limitations and its potentials for statistical analyses, as well as a detailed comparison to that ocean-atmosphere model. The dynamics of DO events in the simple model is depicted in Fig. 3: in the model DO events are regarded as highly nonlinear oscillations between two fundamentally different states of operation, the stacial (“cold”) and the interstadial (“warm”) states. Switches between both model states are assumed to occur each time a given forcing  $f$  (in freshwater flux units, i.e., in milliSverdrup,  $1 \text{ mSv} = 1 \text{ mSverdrup} = 10^3 \text{ m}^3/\text{s}$ ) crosses a certain threshold function  $T$ : a switch from the cold state to the warm state is triggered when the forcing  $f$  falls below a certain threshold value ( $f < T$ ), whereas the opposite switch is assumed to occur when the forcing exceeds the threshold function ( $f > T$ ), cf. Fig. 3. In the model, these switches are regarded as the onset and the termination of a DO event, respectively. During the switches a discontinuity in the threshold function is assumed, i.e.,  $T$  overshoots and after-

ward approaches its respective equilibrium value ( $B_0$  in the stacial state,  $B_1$  in the interstadial state) following a millennial scale relaxation process

$$dT/dt = -(T - B_s)/\tau_s, \quad (1)$$

where  $T$  denotes the threshold function and  $\tau_s$  is the relaxation time in the stacial ( $s=0$ ) and interstadial ( $s=1$ ) model states, respectively.

The dynamics of DO events in the simple two-state model crudely resembles the dynamics of DO events as simulated by a much more sophisticated ocean-atmosphere model of “intermediate complexity,” CLIMBER-2 (Petoukhov *et al.*, 2000; Ganopolski and Rahmstorf, 2001). In that model, whose computational cost is too large to be applicable for extensive statistical analyses on DO events, the events also represent highly nonlinear oscillations in a system with two possible states of operation (corresponding to two fundamentally different modes of buoyancy deep convection in the North Atlantic, cf. Fig. 2), with a threshold and with an overshooting in the stability of the system during the shifts between both model states (Ganopolski and Rahmstorf, 2001; Braun *et al.*, 2007). Analogous to the simple two-state model, shifts from the stacial mode into the interstadial one are triggered by a sufficiently large negative forcing anomaly (i.e., by a reduction in the surface freshwater flux to the northern North Atlantic that exceeds a certain threshold value), and the shifts back into the stacial mode are triggered by a sufficiently large positive forcing anomaly (i.e., by an increase in the freshwater flux that exceeds a certain threshold value). The six free parameters of the simple two-state model (Table II) were estimated from systematic experiments with the ocean-atmosphere model CLIMBER-2, cf. supporting online material in Braun *et al.* (2005) and Braun *et al.* (2007). A detailed comparison between the two models is given in the supplementary material of Braun *et al.* (2007). It is important to emphasize that the simple two-state model is able to reproduce the timing of DO events in the ocean-atmosphere model to a good approximation, which justifies its application for statistical analyses on the timing of DO events.

## III. GHOST STOCHASTIC RESONANCE

In the following we use the simple two-state model to identify characteristics in the recurrence properties of DO events as expected from (i) the proposed GSR scenario and (ii) from a purely random forcing scenario. This step is essential to construct a statistical measure of regularity that has a reasonable power to distinguish between both forcing scenarios. So far measures of periodicity have exclusively been used for that purpose. These measures, however, do not have much power to distinguish between the two scenarios, as has explicitly been demonstrated in a Monte Carlo approach (Braun, 2009). A remedy is to construct more efficient measures of complex regularity, which we will do in Sec. IV. For simplicity we restrict ourselves to highly simplified forcing scenarios with very simple periodic and stochastic forcings and with fixed model parameters. It should be stressed that both the assumed regular solar forcing and the stochastic forcing (which could represent, for example, random fresh-

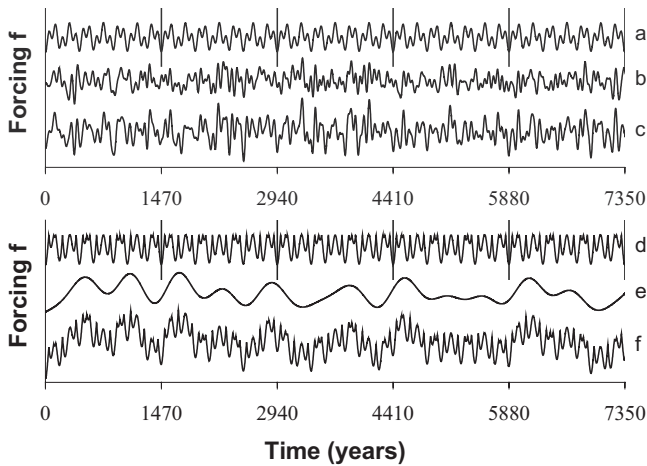


FIG. 4. Forcing in our two considered GSR scenarios. The figure shows the forcing of the simple two-state model. Top: scenario 1 (bisinusoidal periodic input+high-frequency noise). Bottom: scenario 2 (nonsinusoidal periodic input+low-frequency noise). Scenario 1: (a) Bisinusoidal component. This component consists of two added sinusoidal cycles with equal amplitudes  $A$  and with periods  $T_1=1470/17$  ( $\approx 86.5$ ) and  $T_2=1470/7$  ( $=210$ ) yr, respectively, as given by Eq. (2). These periods closely match the leading centennial-scale components of solar activity proxies (Peristykh and Damon, 2003). The bisinusoidal component periodically repeats every 1470 yr, as indicated by the solid lines. (b) Noise component. This component consists of a Gaussian-distributed random signal with a cutoff frequency of  $1/50$   $\text{yr}^{-1}$ . For frequencies lower than  $1/50$   $\text{yr}^{-1}$ , the amplitude of each spectral component is the same and the phase is random. For higher frequencies, the amplitude of each spectral component is zero. (c) Sum of both components. Scenario 2: (d) Nonsinusoidal periodic component. This component consists of a multiplicative combination of two nonsinusoidal cycles with equal amplitudes and with periods  $T_1=1470/7$  and  $T_2=1470/17$  yr, respectively, as given by Eq. (3). Note that the Fourier spectrum of this forcing component [shown in (b) in Braun *et al.* (2005)] exhibits pronounced spectral components with periods  $T_1$  ( $=210$  yr),  $T_2$  ( $\approx 86.5$  yr),  $T_1/2$  ( $=105$  yr),  $T_2/2$  ( $\approx 43.2$  yr),  $T_1 \cdot T_2 / (T_2 + T_1)$  ( $\approx 61.3$  yr), and  $T_1 \cdot T_2 / (T_1 - T_2)$  ( $=147$  yr). These values closely match the leading centennial-scale spectral components in solar activity proxies [shown, for example, in Peristykh and Damon (2003)]. Again, the nonsinusoidal component periodically repeats every 1470 yr, as indicated by the solid lines. (e) Noise signal. This component consists of a Gaussian-distributed random signal with a cutoff frequency of  $1/500$   $\text{yr}^{-1}$ . For frequencies lower than  $1/500$   $\text{yr}^{-1}$ , the amplitude of each spectral component is the same and the phase is random. For higher frequencies, the amplitude of each spectral component is zero. (f) Sum of both components.

water anomalies resulting from internal variability of the continental ice sheets) during the last glacial period are subject to considerable uncertainties and potentially much more complex than the considered forcings in our simplified scenarios. In addition to that, the threshold parameters of glacial climate could also have varied considerably over the course of several DO events. We stress, however, that our focus is the phase distribution of the simulated events in a random forcing scenario and in a GSR scenario, which we find to be fairly stable with respect to modifications in the forcing and model parameters.

To keep our study as simple as possible we first drive the two-state model with a highly simplified GSR forcing, that is, an input  $f$  consisting of two components, cf. top panel in Fig. 4: (i) a bisinusoidal component with equal amplitudes  $A$  and with periods  $T_1=1470/7$  ( $=210$ ) and  $T_2=1470/17$  ( $\approx 86.5$ ) yr, respectively, which means, with cycles close to the main centennial-scale spectral components of solar prox-

ies (Peristykh and Damon, 2003), and (ii) a random Gaussian-distributed component (i.e., noise) with standard deviation  $\sigma$ . A cutoff frequency of the noise of  $1/50$   $\text{yr}^{-1}$  is applied, which means, for spectral components with frequencies higher than  $1/50$   $\text{yr}^{-1}$  the amplitude of the noise term is zero. For lower frequencies the amplitude of each spectral component is the same and the phase is random. This corresponds roughly to a red noise forcing with a correlation time of 50 yr. The total forcing  $f$  is given by the expression

$$f(t) = -A \cos[\omega_1 t] - A \cos[\omega_2 t] + \sigma \cdot n(t), \quad (2)$$

where  $\omega_i = 2\pi/T_i$  and  $n(t)$  denotes the unit variance noise term. In our investigations we consider three different combinations of the forcing parameters  $A$  and  $\sigma$ : (i)  $A=0$  mSv,  $\sigma=7$  mSv, (ii)  $A=5$  mSv,  $\sigma=5$  mSv, and (iii)  $A=7.7$  mSv,  $\sigma=1$  mSv. We note that our bisinusoidal forcing component is certainly highly simplified: 10 000 yr long, tree ring based  $^{14}\text{C}$  records which serve as a standard proxy for solar activity exhibit not only centennial-scale spectral components with periods of about 208 and 88 yr, but also components that correspond apparently to second harmonics ( $\sim 104$  and  $\sim 44$  yr) and combination tones ( $\sim 150$  and  $\sim 60$  yr), compare, for example, Fig. 6(c) in Ogurtsov *et al.* (2002) and Fig. 4 in Peristykh and Damon (2003). These components are convincing indications for a highly nonsinusoidal structure of the centennial-scale solar cycles. We will, therefore, consider a more realistic (i.e., nonsinusoidal) periodic forcing component further below.

From a simulation with the two-state model we calculate the relative frequency of waiting times between successive events in the model output (i.e., the waiting time distribution of the events), as well as the phase distribution as compared with a periodic 1470 yr template. The phase  $\varphi$  of each event is defined as  $\varphi = 2\pi \cdot t / (1470 \text{ yr})$ , where  $t$  denotes the timing of the event (in years). For the chosen forcing parameters  $A$  and  $\sigma$  in the scenarios shown in Fig. 5, the waiting time distribution is centered around a value of about 2940 yr, which corresponds approximately to the average spacing of the DO events 0–10, cf. Table I. We note that the width of the waiting time distribution and also the position of its maximum depend strongly on the parameters of the forcing, for example, on the cutoff frequency and the standard deviation  $\sigma$  of the noise. With a smaller cutoff frequency, a broader waiting time distribution can be obtained (compare Fig. 6), which better resembles the observed waiting time distribution of the 11 DO events in the NGRIP ice core (topmost panel of Figs. 5 and 6). With a larger stochastic forcing, in contrast, the average waiting time between successive events in the simulation decreases, so that for a certain noise level  $\sigma$  the waiting time distribution is centered around a value of 1470 yr, compare Fig. 4 in Braun *et al.* (2008) and Fig. 3 in Braun (2009). In the case without a periodic forcing component the waiting time distribution is smooth and unimodal (top panel of Fig. 5). In the case with a periodic forcing component several modes appear in the distribution, the number of which depends on the signal-to-noise ratio in the forcing (middle and bottom panels in Fig. 5). Note that the position of the modes in the waiting time distribution is solely determined by the general structure of the periodic

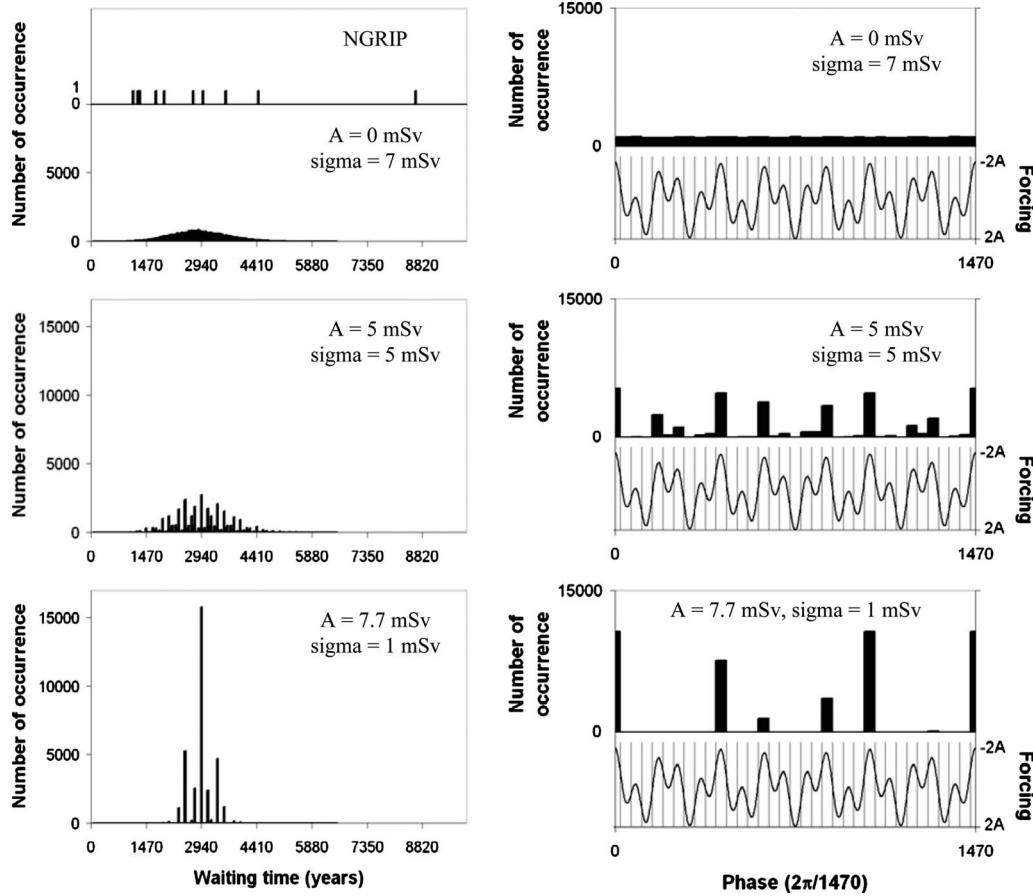


FIG. 5. Recurrence pattern of the simulated DO events in scenario 1. Left: waiting time distribution between successive events in comparison to the distribution as obtained from the 11 events in the NGRIP ice core data (topmost histogram). Right: phase distribution as compared with the periodic bisinusoidal input component. Note that the axis of the forcing is inverted. The signal-to-noise ratio in the forcing increases from top to bottom, as indicated in the respective panels. The 1470 yr phase distribution of the events is uniform in the solely noise-driven case (top) and has an increasingly regular (i.e., multimodal) structure with increasing signal-to-noise ratio in the forcing (middle, bottom). We note that the position of the highest probability maximum in the waiting time distribution is determined by the magnitude of the two forcing parameters  $A$  and  $\sigma$ . In particular, for a different choice of these parameters, the maximum can also be at a value of 1470 yr, corresponding to the period of the bisinusoidal input component.

forcing component, i.e., by the position of the peaks in that component. These peaks result in increased transition rates between the two model states and thus in a preferred tendency of the events to recur with waiting times corresponding to the interpeak time intervals. This effect is more evi-

TABLE I. Timing of the onset of the DO events 0–10 as inferred from the NGRIP deep ice core record from Greenland. The values are in years before 2000 AD and are taken from [Ditlevsen et al. \(2007\)](#).

Event	Timing (before 2000 AD) (yr)
0	11 700
1	14 680
2	23 340
3	27 780
4	28 900
5	32 500
6	33 740
7	35 480
8	38 220
9	40 160
10	41 460

dent from the 1470 yr phase distribution of the simulated events, which is shown in the right part of Fig. 5: in the case without a periodic forcing component (top) the simulated events are purely random and thus do not exhibit a preferred phase relation with the bisinusoidal 1470 yr periodic template. With an increasing signal-to-noise ratio in the forcing, there is an increasing tendency of the simulated events to coincide with the most pronounced extrema in the periodic forcing component. As a result, the 1470 yr phase distribution clearly deviates from a uniform one and shows several peaks (i.e., modes) at values corresponding to the main extrema in the periodic forcing. Quite obviously, this tendency and also the multimodal nature of the phase distribution become more pronounced in the case with a higher signal-to-noise ratio in the forcing (right column of Fig. 5). Accordingly, the number of modes in the 1470 yr phase distribution of the simulated events decreases as the signal-to-noise ratio increases. Note that unlike the waiting time distribution, the simulated phase distribution is fairly insensitive with respect to modification in the parameters of the stochastic forcing component (e.g., its cutoff frequency) and in the spectral composition of the periodic forcing component, compare Figs. 5 and 6. In addition to that, the phase distribution is

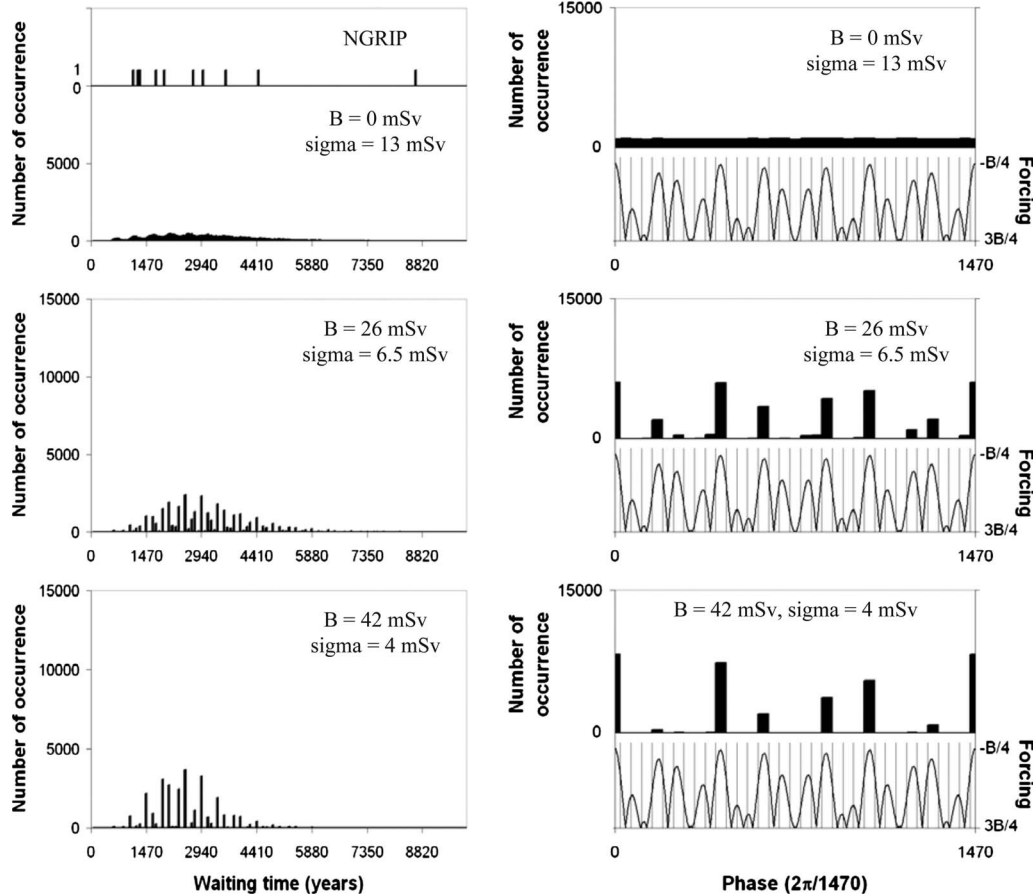


FIG. 6. Recurrence pattern of the simulated DO events in scenario 2. Left: waiting time distribution between successive events in comparison to the distribution as obtained from the 11 events in the NGRIP ice core data (topmost histogram). Right: phase distribution as compared with the periodic nonsinusoidal input component. Note that the axis of the forcing is inverted. The signal-to-noise ratio in the forcing increases from top to bottom, as indicated in the respective panels. The 1470 yr phase distribution of the events is uniform in the solely noise-driven case (top) and has an increasingly regular (i.e., multimodal) structure with increasing signal-to-noise ratio in the forcing (middle, bottom). Note that the parameter values  $B=26$  mSv and  $B=42$  mSv correspond to a standard deviation of the periodic forcing component of about 7.6 and 12.3 mSv, respectively. Again, for a different choice of  $\sigma$  and  $B$ , the highest probability maximum in the waiting time distribution can be at a value of 1470 yr, corresponding to the period of the periodic input component.

also fairly stable with respect to changes in the magnitude of the total forcing, whereas such changes can lead to a strong modification of the simulated waiting time distribution [compare Figs. 5 and 6 with Fig. 3 in Braun (2009)].

To better mimic the apparently highly nonsinusoidal structure of the centennial-scale solar cycles, we further consider a second GSR forcing scenario (bottom panel of Fig. 4), that is, an input  $f$  consisting of (i) a very simple nonsinusoidal component with magnitude  $B$ , and (ii) a random Gaussian-distributed component (i.e., noise) with standard deviation  $\sigma$ . A cutoff frequency of the noise of  $1/500 \text{ yr}^{-1}$  is used. The total forcing  $f$  is given by the expression

$$f(t) = -B \cdot |\cos(\pi t/T_1)| \cdot |\cos(\pi t/T_2)| + 3B/4 + \sigma \cdot n(t) \tag{3}$$

with  $T_1=1470/7$  ( $=210$ ) and  $T_2=1470/17$  ( $\approx 86.5$ ) yr.  $n(t)$  denotes the unit variance noise term. Note that the periodic forcing component exhibits leading spectral components with periods of 210 and  $\sim 86.5$  yr, 105 and  $\sim 43.2$  yr (second harmonics), and 147 and  $\sim 61$  yr (combination tones), compare Fig. 4(b) in Braun *et al.* (2005). These spectral components closely resemble the leading centennial-scale

spectral components in tree ring based  $^{14}\text{C}$  records, a standard proxy for solar activity [compare Fig. 6(c) in Ogurtsov *et al.* (2002) and Fig. 4 in Peristykh and Damon (2003)]. Again, it should be stressed that our implementation of the solar cycles is certainly highly simplified. However, solar activity variations on the centennial scale are subject to considerable uncertainties, in particular, during the last glacial period, so that we do not see any feasible alternative to our approach. In our investigations we consider three different combinations of the forcing parameters  $B$  and  $\sigma$ : (i)  $B=0$  mSv,  $\sigma=13$  mSv, (ii)  $B=26$  mSv,  $\sigma=6.5$  mSv, and (iii)  $B=42$  mSv,  $\sigma=4$  mSv. We note that  $B=26$  mSv and  $B=42$  mSv correspond to a standard deviation of the periodic forcing of about 7.6 and 12.3 mSv, respectively.

From a simulation with the two-state model we again calculate the waiting time distribution of the events as well as the phase distribution as compared with a periodic 1470 yr template. The phase  $\varphi$  of each event is defined as  $\varphi = 2\pi \cdot t / (1470 \text{ yr})$ , where  $t$  denotes the timing of the event (in years). For the chosen forcing parameters  $B$  and  $\sigma$  in the scenarios shown in Fig. 6, the waiting time distribution is centered around a value of slightly less than 2940 yr, which

corresponds approximately to the average spacing of the DO events 0–10, cf. Table I. In the case without a periodic forcing component, the waiting time distribution is again smooth (top panel of Fig. 6). But in the case with a periodic forcing component, several modes appear in the distribution, the number of them depends on the signal-to-noise ratio in the forcing (middle and bottom panels of Fig. 6). Note that the waiting time distributions in Fig. 6 are somewhat broader than the ones in Fig. 5, which is in better agreement with the NGRIP data and results mainly from the lower cutoff frequency in Fig. 6. Apart from that, the position of the modes in the waiting time distribution is similar to Fig. 5. Again, the phase distribution of the simulated events (right part of Fig. 6) is uniform in the absence of a periodic forcing component. With an increasing signal-to-noise ratio in the forcing, there is also an increasing tendency of the simulated events to coincide with the most pronounced extrema in the periodic forcing component. As a result, the 1470 yr phase distribution clearly deviates from a uniform one and again shows several peaks (i.e., modes) at values corresponding to the main extrema in the periodic forcing. As before, this tendency and also the multimodal nature of the phase distribution become more pronounced in the case with a higher signal-to-noise ratio in the forcing (right panels of Fig. 6). Accordingly, the number of modes in the 1470 yr phase distribution of the simulated events decreases as the signal-to-noise ratio increases.

Note that several characteristic time scales exist in our model simulations, i.e., the periods  $T_1=1470/7$  yr and  $T_2=1470/17$  yr of the two centennial-scale forcing cycles, the fundamental period  $T=1470$  yr of the periodic forcing, the inverse of the cutoff frequency of the stochastic forcing, the average waiting time between successive DO events, and the millennial relaxation times  $\tau_1$  and  $\tau_2$  of the applied model. All these time scales are reflected in the recurrence properties of the simulated DO events: the existence of the relaxation times  $\tau_1$  and  $\tau_2$ , for example, which represent the characteristic time scale on which the density-driven (i.e., “thermohaline”) ocean circulation is thought to converge from a nonequilibrium configuration toward its equilibrium state, confines the waiting time distribution of the simulated events to a much narrower range than would be obtained in the case of a constant threshold, as discussed by Braun *et al.* (2007). The width of the waiting time distribution is also affected by the choice of the cutoff frequency of the stochastic forcing, with a higher cutoff frequency leading to a narrower distribution (compare left columns in Figs. 5 and 6). Moreover, the maximum of highest probability in the waiting time corresponds approximately to the average spacing between successive DO events in the simulation and depends on both the noise intensity  $\sigma$  and the magnitude of the periodic forcing. In contrast, the position of the different modes in the waiting time distribution and in the 1470 yr phase distribution is exclusively determined by the position of the peaks in the periodic forcing (compare right columns of Figs. 5 and 6) and thus by the periods  $T_1$ ,  $T_2$ , and  $T$  of this forcing component, while the magnitude of the modes in the waiting time distribution is also affected by the other time scales,

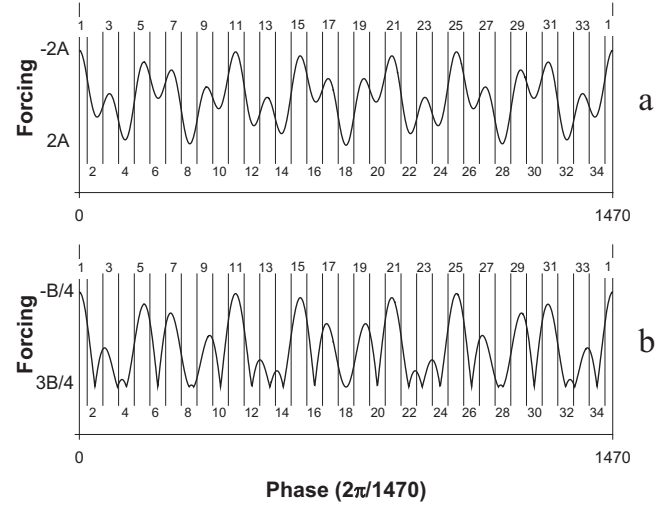


FIG. 7. Definition of our measures of regularity. To define our measures we divide the 1470 yr fundamental period of the periodic forcing into 34 bins, each centered around the 34 positive and negative extrema of the 1470/17 yr spectral component (as labeled by the numbers 1–34 in the figure). Note that the same binning is used in the scenario with the (a) bisinusoidal forcing and the (b) nonsinusoidal forcing. Each event is then placed into one bin, according to the timing of its onset. The total number of events in the most frequently populated one/two/three bins yields our measures of complex regularity. For more information see text.

e.g., by the choice of the cutoff frequency (compare left columns of Figs. 5 and 6).

#### IV. MEASURES OF MULTIMODALITY

In this section we first define new measures of phase multimodality. Based on our model simulations, we then demonstrate the ability of these measures to distinguish between a scenario of solely noise-induced DO events and a GSR scenario on the basis of only 11 events. Finally we apply our measures to analyze the recurrence pattern of DO events in the NGRIP ice core from Greenland.

Let  $t_i$  ( $i \in [1, 11]$ ) be the timing of the  $i$ th DO event in the model simulation and  $T=1470$  yr the period of the prescribed periodic forcing component. We then define

$$\varphi_i = t_i \bmod T \quad (4)$$

as the phase of the  $i$ th event compared with the periodic forcing component ( $\varphi_i \in [0, 1469]$ ). Now we divide the possible range of  $\varphi_i$ -values into 34 ( $=1470 \text{ yr}/[86.5 \text{ yr}/2]$ ) bins of equal width, which are centered around the positive and negative forcing anomalies, as depicted in Fig. 7. Each of the 11 DO events is then placed into one of the 34 bins (which we label  $j$ ;  $j \in [1, 34]$ ), according to the timing of its onset. Our choice of the number of bins is simply the number of positive and negative peaks in the prescribed  $\sim 86.5$  yr spectral component of the periodic forcing. Finally we define  $n_j$  as the number of events that fall within the  $j$ th bin. Obviously,  $n_j$  lies between zero and eleven for each value of  $j$ , and  $n_1 + \dots + n_{34} = 11$  since we consider a total number of 11 DO events. Based on these quantities, we define three different measures of regularity,

$$M_1 = \max n_j (j \in [1, 34]), \quad (5)$$

$$M_2 = \max n_j + n_k (j, k \in [1, 34]; j \neq k), \quad (6)$$

$$M_3 = \max n_j + n_k + n_l (j, k, l \in [1, 34]; l \neq j, k). \quad (7)$$

Thus,  $M_1$  corresponds to the maximum number of events in one single bin,  $M_2$  denotes the sum of events in the two most frequently populated bins, and  $M_3$  labels the sum of events in the three most frequently populated bins. As one can already see from Figs. 5 and 6 (right part), these three measures of complex regularity are likely to exhibit small values in a scenario of solely noise-induced DO events, whereas they will typically have much larger values in a GSR scenario with a high signal-to-noise ratio. This justifies our choice of these three measures to distinguish between the two forcing scenarios. It should be stressed that apart from the number of bins each measure contains two adjustable parameters, that is, the period  $T$  of the 1470 yr periodic forcing component and the relative position of the bins compared with the periodic forcing (i.e., the phase  $\varphi_0$  of the bins compared with the forcing). In contrast to our model study, in which the optimal choice of these parameters is obvious, the existence of these parameters must be taken into account when analyzing the recurrence pattern of DO events in paleoclimatic records, because the dating uncertainties of the records impose uncertainties on the optimal choice of these parameters.

We now quantitatively test the performance of our three measures by means of a Monte Carlo simulation. This is done as follows: using the simple two-state model from Sec. II, we simulate 3000 realizations of a series containing 11 DO events, for each combination of the forcing parameters, as denoted in Sec. III. In each of the 3000 realizations we then calculate the values obtained for the measures, which gives us their distribution in the considered forcing scenarios (Figs. 8 and 9). In the solely noise-induced case we further distinguish two methodologically different approaches: in the first approach [Figs. 8(a)–8(c) and Figs. 9(a)–9(c)] we consider the position of the 34 bins as fixed, as depicted in Fig. 7. In the second approach [Figs. 8(d)–8(f) and Figs. 9(d)–9(f)] we treat the relative position of the bins as tunable. That means, in any single realization we allow for a uniform shifting of all bins in the phase domain, such that this shift results in a maximization of the measures. As a result of this optimization, the simulated probability distribution is shifted toward slightly higher values as compared with the untuned case.

From Figs. 8 and 9 it is evident that the distributions of the three measures differ notably when the signal-to-noise ratio in the forcing is altered. For example, in the purely noise-driven scenario the probability to find four or more events in the most frequently populated bin (i.e.,  $M_1 \geq 4$ ) is smaller than 0.03 [Fig. 8(d)]. In the GSR scenario with the highest signal-to-noise ratio, in contrast, the probability to find three or less events in the most frequently populated bin (i.e.,  $M_1 \leq 3$ ) is smaller than 0.05 [Fig. 8(j)]. Thus, in order to distinguish between these two model scenarios, a simple one-sided test could be constructed, in which the null hypothesis of purely noise-driven events is rejected if and only if  $M_1 \geq 4$ . This test would be fairly efficient with a significance level of about 0.97 and a power of about 0.95. A

one-sided test with the measures  $M_2$  and  $M_3$  as test statistics would be even more efficient with a significance level of  $\sim 0.98$  and a power of more than 0.99 (rejection of the null hypothesis if and only if  $M_2 \geq 6$ ; cf. Figs. 8(e) and 8(k)), respectively, 0.99 and more than 0.99 (rejection of the null hypothesis if and only if  $M_3 \geq 8$ ; cf. Figs. 8(f) and 8(l)). The high efficiency of the tests is also evident from the fact that the corresponding distributions of our three measures in the considered model scenarios are almost disjunct (Fig. 8). Applying the same tests to the scenarios shown in Fig. 9, that is, to the solely noise-induced scenario [Figs. 9(d)–9(f)] and the GSR scenario with the highest signal-to-noise ratio [Figs. 9(j)–9(l)], gives qualitatively similar results with a significance of  $\sim 0.98$  and a power of  $\sim 0.78$  ( $M_1 \geq 4$ ),  $\sim 0.98$ , and  $\sim 0.97$  ( $M_2 \geq 6$ ), respectively,  $\sim 0.99$  and  $\sim 0.95$  ( $M_3 \geq 8$ ). Accordingly, it is possible to distinguish with high confidence between solely noise-induced DO events on one hand (first and second rows) and a GSR scenario with a high signal-to-noise ratio on the other hand (bottom row), even on the basis of only 11 DO events, as we also explicitly tested with the Kolmogorov–Smirnov test. Moreover, it is also possible to distinguish with at least some confidence between these two extreme cases on one hand and a GSR scenario with an intermediate signal-to-noise ratio on the other hand. Thus, our measures of complex regularity are apparently applicable for the analysis of DO events in paleoclimatic records, e.g., in deep ice core records from Greenland.

We note that not only a GSR mechanism has been proposed to explain the recurrence pattern of DO events, but also a CR (Timmermann *et al.*, 2003) and a SR (Alley *et al.*, 2001) mechanism. For a SR mechanism, however, a regular driver with a leading millennial-scale frequency is required, which is not known. In the context of DO events, we thus do not see the relevance to distinguish between a SR and a GSR mechanism. We further note that a CR mechanism (Pikovsky and Kurths, 1997) does not occur in our model of DO events, at least not with the choice of the model parameters as given in Table II. While it might be of more relevance to test the power of our measures to distinguish between a GSR and a CR mechanism, this test is, thus, not possible in the framework of our model. To perform such a test, a fundamentally different model of DO events would therefore be required, which is beyond the scope of this paper. Having shown the applicability of our measures for statistical hypothesis testing, we now use these measures for a first analysis of DO events in the NGRIP ice core from Greenland (Fig. 1). This is done as follows: using the timing of the onset of the DO events 0–10 as given in Table I, we maximize the three measures  $M_1$ ,  $M_2$ , and  $M_3$  by optimizing the two free parameters  $T$  and  $\varphi_0$  of the binning over some range. More precisely, the phase  $\varphi_0$  is optimized over all possible values. The period  $T$  is optimized over the somewhat arbitrary range of 1000–2000 yr. For a period of 1487–1488 yr we find a pronounced maximum in the values of all three of our measures with  $M_1=5$ ,  $M_2=9$ , and  $M_3=10$ , cf. right part in Fig. 1. Figure 10(a) shows that within the considered range of 1000–2000 yr all measures take a global maximum at  $T=1488$  yr, which exceeds the standard range of variability in the distribution of our measures by up to three units. We further tested

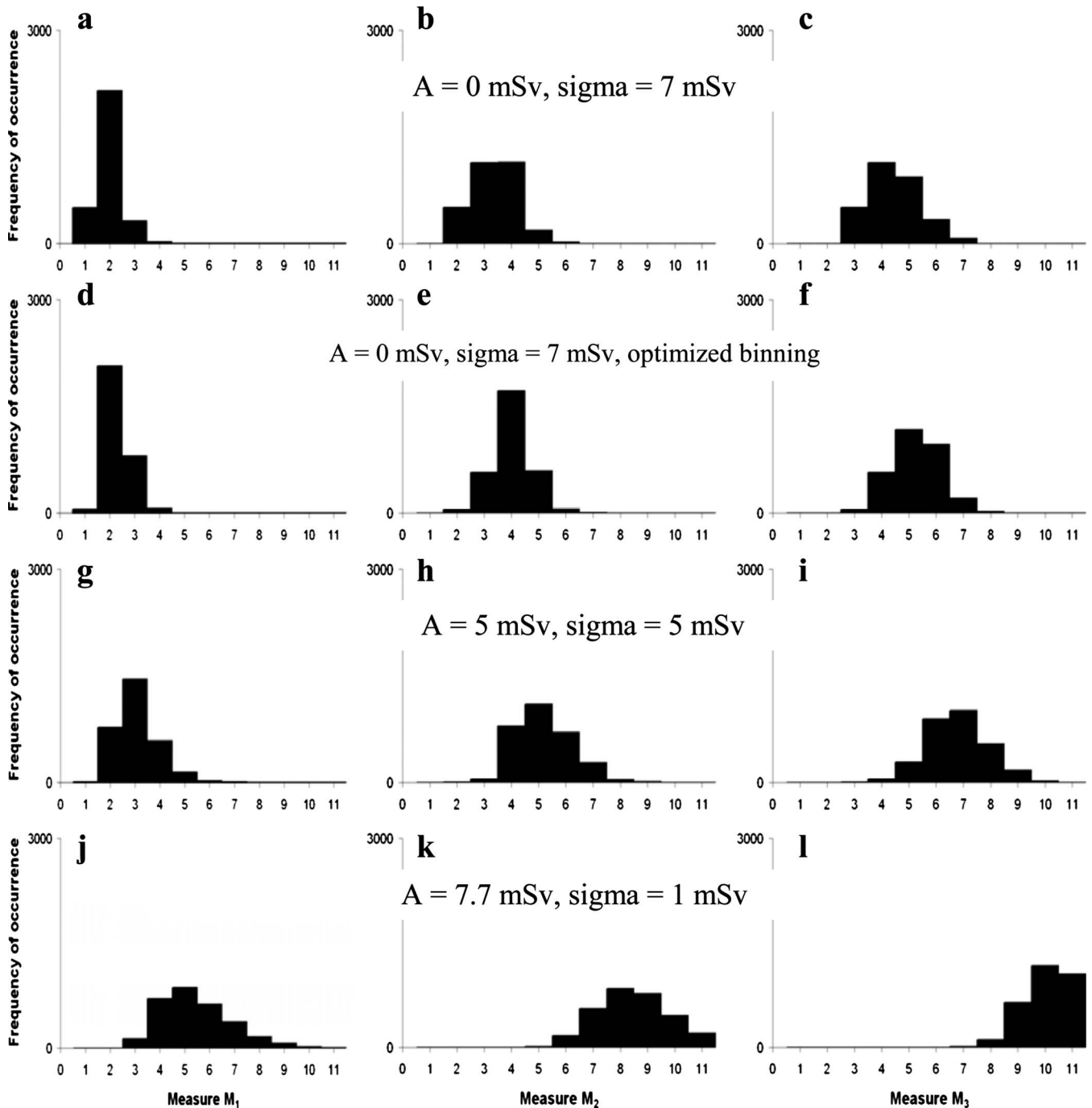


FIG. 8. Performance of our statistical measures in scenario 1. The figure shows the distribution of the measures  $M_1$  (left),  $M_2$  (middle), and  $M_3$  (right) for three different signal-to-noise ratios in the forcing with increasing signal-to-noise level from top to bottom. In each realization the value of the measures as obtained from a series of 11 DO events is calculated. The ensemble size is 3000 realizations. Note that the distributions in the first [(a)–(c)], third [(g)–(i)], and fourth [(j)–(l)] rows were calculated with a fixed position of the bins, as shown in Fig. 7. In the distributions in the second row [(d)–(f)], in contrast, the position of the bins has been treated as tunable and has been optimized in a way to maximize the coincidence of the events with the bins (see text for more details). All three measures have a reasonable power to distinguish between the considered forcing scenarios. The number of bins is 34, as illustrated in Fig. 7.

the stability of this global maximum with respect to modifications in the number of bins in our measures of regularity [Fig. 10(b)]. As can be seen from the figure, using even a considerably different number of bins has little impact on our results, which further strengthens our findings. We also investigated the distribution of our measures as a function of the chosen reference phase of the bins [Fig. 10(c)]. The figure shows that all measures take their maximum values within a continuous range of bin phases, which is precisely

the same range for all three measures. Consequently, our results are also stable with respect to changes in the exact bin location. A comparison to the simulated distributions of the three measures, as shown in Figs. 8 and 9, indicates that the observed values are consistent with a GSR scenario, and even agree with a very high signal-to-noise ratio in the forcing. We note that between the DO events 2 and 3 in the NGRIP ice core, the waiting time is about 8660 yr. This value is very unlikely according to the waiting time distribu-

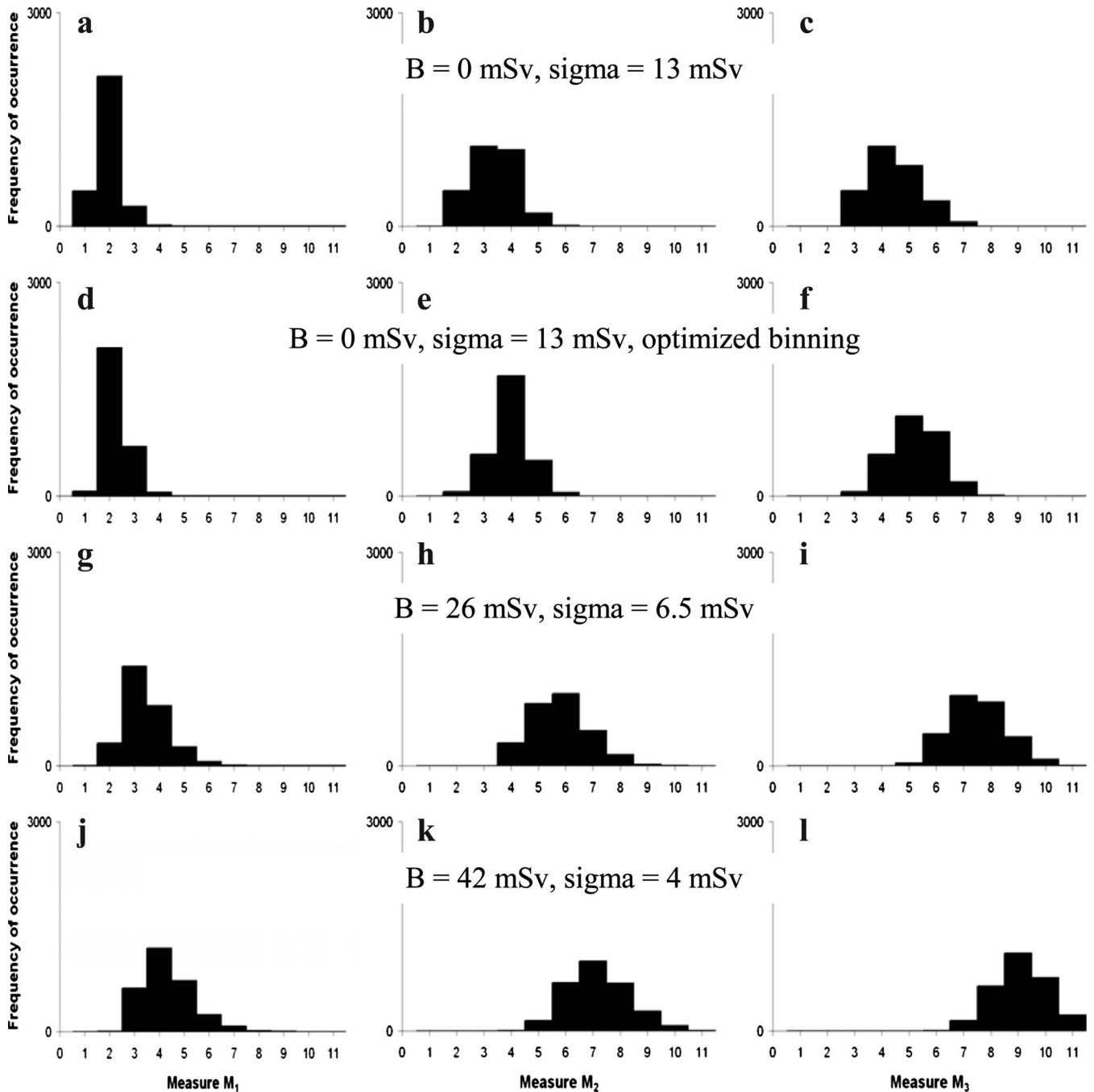


FIG. 9. Performance of our statistical measures in scenario 2. The figure shows the distribution of the measures  $M_1$  (left),  $M_2$  (middle), and  $M_3$  (right) for three different signal-to-noise ratios in the forcing with increasing signal-to-noise level from top to bottom. In each realization the value of the measures as obtained from a series of 11 DO events is calculated. The ensemble size is 3000 realizations. Note that the distributions in the first [(a)–(c)], third [(g)–(i)], and fourth [(j)–(l)] rows were calculated with a fixed position of the bins, as shown in Fig. 7. In the distributions in the second row [(d)–(f)], in contrast, the position of the bins has been treated as tunable and has been optimized in a way to maximize the coincidence of the events with the bins (see text for more details). The number of bins is 34, as illustrated in Fig. 7.

tions shown in Fig. 5. According to the distributions shown in the top and middle parts of Fig. 6, however, similarly large values ( $>8000$  yr) still have a non-negligible probability of occurrence at least once in a series of 11 events, with an approximate probability of 5% in the upper panel of Fig. 6 and 2.5% in the middle panel. This possible mismatch between the simulated distributions and the ice core data is not taken into account when calculating the three measures in

Figs. 8 and 9, since we only look at the waiting times modulo of 1470 yr.

It should be stressed, however, that we are not yet able to estimate the statistical significance of the detected recurrence pattern. In particular, it is not yet possible to estimate the statistical significance of the detected pattern based on the simulated distributions of our three measures of regularity, as shown in Figs. 8(d)–8(f) and Figs. 9(d)–9(f), since these

TABLE II. Parameters of the simple two-state model. Values of  $A_0$ ,  $A_1$ ,  $B_0$ , and  $B_1$  are in milliSverdrup ( $1 \text{ mSv} = 1 \text{ mSverdrup} = 10^3 \text{ m}^3/\text{s}$ ), that it is freshwater flux units, since the model was originally designed to mimic the response of an ocean-atmosphere model to a given freshwater anomaly in the northern North Atlantic. Note that these parameter values are identical to the values used in the original version of the two-state model, cf. supplementary material in [Braun et al. \(2005\)](#). For these values it was shown that the two-state model is able to mimic the dynamical principles of DO events as simulated with a much more comprehensive ocean-atmosphere model of intermediate complexity ([Braun et al., 2007](#)).

Parameter	Value
$A_0$	-27 mSv
$A_1$	27 mSv
$B_0$	-9.7 mSv
$B_1$	11.2 mSv
$\tau_0$	1200 yr
$\tau_1$	800 yr

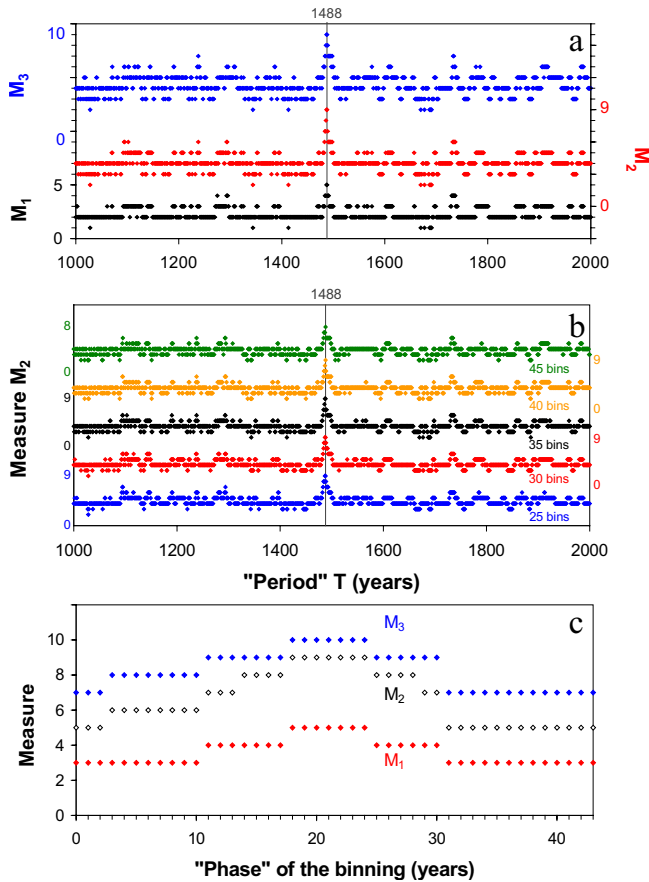


FIG. 10. (Color online) Analysis of the DO events 0–10 in the NGRIP ice core by means of our three measures of regularity. The timing of the 11 events is given in Table I. The figure shows (a) the distribution of the three measures ( $M_1$ ,  $M_2$ , and  $M_3$ ) as a function of the template “period”  $T$ . We use 34 bins, as illustrated in Fig. 7. For each value of  $T$  the phase of the template has been optimized in order to maximize our measures. Note that all measures take their global maximum at a value  $T = 1488$  yr. (b) The distribution of the measure  $M_2$  as a function of the template period  $T$  for different choices of the number of bins. Each curve corresponds to a different number of bins, as indicated in the figure. Again, the phase of the template has been optimized. Note that all curves take their global maximum at  $T = 1488$  yr. (c) The distribution of the three measures as a function of the template phase (in years). We use 34 bins and a template period  $T = 1488$  yr, which results in a possible range of  $1488/34$  ( $\approx 43$ ) different template phases. Note that all curves take their global maximum at the same range of template phases.

were simulated for one given value of the free parameter  $T$  (i.e., the period) of our measures. When analyzing the ice core data, in contrast, the parameter  $T$  must be regarded as tunable at least within a range that is determined by the uncertainty in both the ice core chronology and the solar cycle periods. A remedy is to maximize the measures over both parameters  $T$  and  $\varphi_0$ , and not just over  $\varphi_0$ , as was done in Figs. 8(d)–8(f) and Figs. 9(d)–9(f). Such a treatment, however, is more complicated since it requires the specification of an objective range of  $T$ -values over which the measures are maximized, and is thus beyond the scope of this paper. We further note that the chosen bin size of our measures (1470/34 yr; that means, 3% of 1470 yr) is comparable to the estimated dating uncertainty of the NGRIP ice core chronology ([Andersen et al., 2006](#)). With our measures we thus operate near the dating limit of the ice core record.

## V. CONCLUSIONS

In this paper three new statistical measures of complex regularity (that is, of phase multimodality) were constructed. Using a Monte Carlo approach with a simple two-state model of glacial climate switches, the DO events, we demonstrated the ability of the measures to distinguish between a GSR and a solely noise-induced resonance on the basis of just 11 events. Finally we applied our measures to analyze the recurrence pattern of DO events in a deep ice core from Greenland, and we observed a pattern that is consistent with a GSR. Further work is needed to estimate the statistical significance of the detected recurrence pattern and to use these measures for time series analysis of DO events in other paleoclimatic records.

## ACKNOWLEDGMENTS

H.B. was funded by the German Research Foundation (DFG), Project No. BR 3911/1-1. J.K. was funded by SFB 555, project C1 (DFG).

- Alley, R., Marotzke, J., Nordhaus, W., Overpeck, J., Peteet, D., Pielke, R., Jr., Pierrehumbert, R., Rhines, P., Stocker, T., Talley, L., and Wallace, J., “Abrupt climate change,” *Science* **299**, 2005–2010 (2003).
- Alley, R. B., Anandakrishnan, S., and Jung, P., “Stochastic resonance in the North Atlantic,” *Paleoceanography* **16**, 190–198 (2001).
- Alley, R. B. and Clark, P. U., “The deglaciation of the northern hemisphere: A global perspective,” *Annu. Rev. Earth Planet Sci.* **27**, 149–182 (1999).
- Andersen, K., Svensson, A., Johnsen, S. J., Rasmussen, S. O., Bigler, M., Röthlisberger, R., Ruth, U., Siggaard-Andersen, M.-L., Steffensen, J. P., Dahl-Jensen, D., Vinther, B. M., and Clausen, H. B., “The Greenland ice core chronology 2005, 15–42 ka. Part 1: Constructing the time scale,” *Quat. Sci. Rev.* **25**, 3246–3257 (2006).
- Boccaletti, S., Kurths, J., Osipov, G., Valladares, D. L., and Zhou, C. S., “The synchronization of chaotic systems,” *Phys. Rep.* **366**, 1–101 (2002).
- Bond, G., Broecker, W., Johnsen, S., McManus, J., Labeyrie, L., Jouzel, J., and Bonani, G., “Correlations between climate records from North Atlantic sediments and Greenland ice,” *Nature (London)* **365**, 143–147 (1993).
- Braun, H., “Measures of periodicity for time series analysis of threshold-crossing events,” *Eur. Phys. J. Spec. Top.* **174**, 33–47 (2009).
- Braun, H., Christl, M., Rahmstorf, S., Ganopolski, A., Mangini, A., Kubatzki, C., Roth, K., and Kromer, B., “Possible solar origin of the 1470-year glacial climate cycle demonstrated in a coupled model,” *Nature (London)* **438**, 208–211 (2005).
- Braun, H., Ditlevsen, P. D., and Chialvo, D. R., “Solar forced Dansgaard-

- Oeschger events and their phase relation with solar proxies," *Geophys. Res. Lett.* **35**, L06703, doi:10.1029/2008GL033414 (2008).
- Braun, H., Ganopolski, A., Christl, M., and Chialvo, D. R., "A simple conceptual model of abrupt glacial climate events," *Nonlinear Processes Geophys.* **14**, 709–721 (2007).
- Broecker, W. S., Peteet, D. M., and Rind, D., "Does the ocean-atmosphere system have more than one stable mode of operation?," *Nature (London)* **315**, 21–26 (1985).
- Dansgaard, W., Clausen, H. B., Gundestrup, N., Hammer, C. U., Johnsen, S. F., Kristinsdottir, P. M., and Reeh, N., "A new Greenland deep ice core," *Science* **218**, 1273–77 (1982).
- Ditlevsen, P. D., Andersen, K. K., and Svensson, A., "The DO-climate events are probably noise induced: Statistical investigation of the claimed 1,470 years cycle," *Clim. Past* **3**, 129–134 (2007).
- Ditlevsen, P. D. and Ditlevsen, O. D., "On the stochastic nature of the rapid climate shifts during the last ice age," *J. Clim.* **22**, 446–457 (2009).
- Ditlevsen, P. D., Kristensen, M. S., and Andersen, K. K., "The recurrence time of Dansgaard-Oeschger events and possible causes," *J. Clim.* **18**, 2594–2603 (2005).
- Feynman, J. and Fougere, P. F., "Eighty-eight year periodicity in solar-terrestrial phenomena confirmed," *J. Geophys. Res.* **89**, 3023–3027, doi:10.1029/JA089iA05p03023 (1984).
- Ganopolski, A. and Rahmstorf, S., "Simulation of rapid glacial climate changes in a coupled climate model," *Nature (London)* **409**, 153–158 (2001).
- Groote, P. M., Stuiver, M., White, J. W. C., Johnsen, S., and Jouzel, J., "Comparison of oxygen isotope records from the GISP2 and GRIP Greenland ice cores," *Nature (London)* **366**, 552–554 (1993).
- Lang, C., Leuenberger, M., Schwander, J., and Johnsen, S., "16 °C rapid temperature variation in central Greenland 70,000 years ago," *Science* **286**, 934–937 (1999).
- Oeschger, H., Beer, J., Siegenthaler, U., Stauffer, B., Dansgaard, W., and Langway, C. C., "Late glacial climate history from ice cores," in *Climate Processes and Climate Sensitivity*, Geophysical Monograph Series Vol. 5, edited by Hansen, J. E. and Takahashi, T. (AGU, Washington, DC, 1984), pp. 299–306.
- Ogurtsov, M. G., Nagovitsyn, Y. A., Kocharov, G. E., and Jungner, H., "Long-period cycles of the Sun's activity recorded in direct solar data and proxies," *Sol. Phys.* **211**, 371–394 (2002).
- Peristykh, A. N. and Damon, P. E., "Persistence of the Gleissberg 88-yr solar cycle over the last 12,000 years: Evidence from cosmogenic isotopes," *J. Geophys. Res.* **108**, SSH 1-1–SSH 1-15, doi:10.1029/2002JA009390 (2003).
- Petoukhov, V., Ganopolski, A., Brovkin, V., Claussen, M., Eliseev, A., Kutzbach, C., and Rahmstorf, S., "CLIMBER-2: A climate system model of intermediate complexity. Part I: Model description and performance for present climate," *Clim. Dyn.* **16**, 1–17 (2000).
- Pikovsky, A. S. and Kurths, J., "Coherence resonance in a noise-driven excitable system," *Phys. Rev. Lett.* **78**, 775–778 (1997).
- Rahmstorf, S., "Timing of abrupt climate change: A precise clock," *Geophys. Res. Lett.* **30**, 17-1–17-4, doi:10.1029/2003GL017115 (2003).
- Sarnthein, M., Winn, K., Jung, S. J. A., Duplessy, J. C., Labeyrie, L., Erlenkeuser, H., and Ganssen, G., "Changes in East Atlantic deepwater circulation over the last 30,000 years: Eight time slice reconstructions," *Paleoceanography* **9**, 209–267 (1994).
- Schulz, M., "On the 1,470-year pacing of Dansgaard-Oeschger warm events," *Paleoceanography* **17**, 4-1–4-9 (2002).
- Severinghaus, J. P. and Brook, E., "Abrupt climate change at the end of the last glacial period inferred from trapped air in polar ice," *Science* **286**, 930–934 (1999).
- Steffensen, J. P., Andersen, K. K., Bigler, M., Clausen, H. B., Dahl-Jensen, D., Fischer, H., Goto-Azuma, K., Hansson, M., Johnsen, S. J., Jouzel, J., Masson-Delmotte, V., Popp, T., Rasmussen, S. O., Röthlisberger, R., Ruth, U., Stauffer, B., Siggaard-Andersen, M. L., Sveinbjörnsdottir, A. E., Svensson, A., and White, J. W. C., "High-resolution Greenland ice core data show abrupt climate change happens in few years," *Science* **321**, 680–684 (2008).
- Stuiver, M. and Braziunas, T. F., "Sun, ocean, climate and atmospheric CO<sub>2</sub>: An evaluation of causal and spectral relationships," *Holocene* **3**, 289–305 (1993).
- Svensson, A., Andersen, K. K., Bigler, M., Clausen, H. B., Dahl-Jensen, D., Davies, S. M., Johnsen, S. J., Muscheler, R., Rasmussen, S. O., Röthlisberger, R., Steffensen, J. P., and Vinther, B. M., "The Greenland ice core chronology 2005, 15–42 ka. Part 2: Comparison to other records," *Quat. Sci. Rev.* **25**, 3258–3267 (2006).
- Timmermann, A., Gildor, H., Schulz, M., and Tziperman, E., "Coherent resonant millennial-scale climate oscillations triggered by massive melt-water pulses," *J. Clim.* **16**, 2569–2585 (2003).